ISSN 1674-1056
http://cpb.iphy.ac.cn
http://iopscience.iop.org/cpb
中国物理 B
Chinese Physics
中国物理 Chinese Physics B

Ghost images reconstructed from fractional-order moments with thermal light

De-Zhong Cao(曹德忠), Qing-Chen Li(李清晨), Xu-Cai Zhuang(庄绪财), Cheng Ren(任承), Su-Heng Zhang(张素恒), Xin-Bing Song(宋新兵)

Citation: Chin. Phys. B . 2018, 27(12): 123401. **doi:** 10.1088/1674-1056/27/12/123401
Journal homepage: http://cpb.iphy.ac.cn; http://iopscience.iop.org/cpb

What follows is a list of articles you may be interested in

Reflective ghost imaging free from vibrating detectors

Heng-xing Li(李恒星), Yan-feng Bai(白艳锋), Xiao-hui Shi(施晓辉), Su-qin Nan(南苏琴), Li-jie Qu(屈利杰), Qian Shen(沈倩), Xi-quan Fu(傅喜泉)

Chin. Phys. B . 2017, 26(10): 104204. **doi:** 10.1088/1674-1056/26/10/104204

Optical encryption scheme based on ghost imaging with disordered speckles

Yu-dong Zhang(张玉东), Sheng-mei Zhao(赵生妹)

Chin. Phys. B . 2017, 26(5): 054205. **doi:** 10.1088/1674-1056/26/5/054205

Increasing the range accuracy of three-dimensional ghost imaging ladar using optimum slicing number method

Yang Xu, Zhang Yong, Xu Lu, Yang Cheng-Hua, Wang Qiang, Liu Yue-Hao, Zhao Yuan

Chin. Phys. B . 2015, 24(12): 124202. **doi:** 10.1088/1674-1056/24/12/124202

Ghost imaging with broad distance

Duan De-Yang, Zhang Lu, Du Shao-Jiang, Xia Yun-Jie

Chin. Phys. B . 2015, 24(10): 104203. **doi:** 10.1088/1674-1056/24/10/104203

Dynamical effects of the four-wave mixing enhancement induced by constructive quantum interference

Xue Yan, Wang Gang, Wu Jin-Hui, Zhang Bing, Gao Jin-Yue

Chin. Phys. B . 2011, 20(3): 033403. **doi:** 10.1088/1674-1056/20/3/033403

Ghost images reconstructed from fractional-order moments with thermal light*

De-Zhong Cao(曹德忠)[1,†], Qing-Chen Li(李清晨)[1], Xu-Cai Zhuang(庄绪财)[1], Cheng Ren(任承)[1], Su-Heng Zhang(张素恒)[2], and Xin-Bing Song(宋新兵)[3,‡]

[1] *Department of Physics, Yantai University, Yantai* 264005, *China*
[2] *College of Physics Science and Technology, Hebei University, Baoding* 071002, *China*
[3] *Department of Physics of Complex Systems, Weizmann Institute of Science, Rehovot* 76100, *Israel*

(Received 29 July 2018; revised manuscript received 30 September 2018; published online 10 November 2018)

We present the joint probability density function (PDF) between the bucket signals and reference signals in thermal light ghost imaging, by regarding these signals as stochastic variables. The joint PDF allows us to examine the fractional-order moments of the bucket and the reference signals, in which the correlation orders are fractional numbers, other than positive integers in previous studies. The experimental results show that various images can be reconstructed from fractional-order moments. Negative (positive) ghost images are obtained with negative (positive) orders of the bucket signals. The visibility and peak signal-to-noise ratios of the diverse ghost images depend greatly on the fractional orders.

Keywords: ghost imaging, intensity correlation function, fractional-order moments

PACS: 34.80.Pa, 42.30.–d **DOI:** 10.1088/1674-1056/27/12/123401

1. Introduction

High-order correlation measurement is an important tool for image acquisition between correlated systems. In the system of thermal light ghost imaging (TLGI),[1–7] the object information is reconstructed by measuring the intensity correlation functions between the bucket (object) signals and reference signals. From the viewpoint of probability theory, these correlation functions $\langle I_{\rm B}^{\mu} I_{\rm r}^{\nu} \rangle$ are the joint moments of the bucket signals $I_{\rm B}$ and reference signals $I_{\rm r}$. In the previous investigations, all of the correlation orders (μ and ν) were positive integers. The most favorite choice was $\mu = \nu = 1$. In 2006, TLGI without lenses[8,9] was proposed and investigated by two groups. Computational TLGI[10] was performed with just bucket signals by Shapiro in 2008. Recently, TLGI was applied to remote sensing,[11] lidar,[12,13] imaging encryption,[14] and biomedical imaging.[15] The higher integer-order intensity correlation functions were proposed to enhance the visibility degree[16] and to improve the contrast-to-noise ratios[17,18] of the ghost images.

The positive integer orders are no longer suitable in certain circumstances. For examples, the fractional-order moments must be considered in processes such as truncated Lévy flights[19] and atmospheric laser scintillations.[20] In this paper, we investigate the fractional-order moments, where the orders μ and ν are fractional numbers, between the bucket and reference signals in TLGI systems. The crucial step for fractional-order moments in our theory is to determine the precise joint probability density function (PDF) $P_2(I_{\rm B}, I_{\rm r})$ between the bucket signals and reference signals. The object information can be reconstructed with the fractional-order moments

$$\langle I_{\rm B}^{\mu} I_{\rm r}^{\nu} \rangle = \iint I_{\rm B}^{\mu} I_{\rm r}^{\nu} \times P_2(I_{\rm B}, I_{\rm r}) \, {\rm d}I_{\rm B} \, {\rm d}I_{\rm r} \tag{1}$$

for any arbitrary correlation orders.

In real experiments, the orders of the reference signals are set positive to avoid infinity, while the orders of the bucket signals can be positive or negative fractional numbers. We find that negative (positive) ghost images are obtained in measuring fractional-order moments with negative (positive) orders of the bucket signals. The visibility degrees and signal-to-noise ratios (SNRs) of the ghost images vary with the fractional orders. In this paper, the fractional-order moments in TLGI are examined in an experiment with a binary object. Advertise ghost images are reconstructed by measuring fractional-order moments of the stochastic bucket and reference intensity signals. Since the correlation orders are not restricted within integers, the visibility and SNR of the ghost images can be controlled in a delicate way.

2. Joint probability density function between the bucket and reference signals

Figure 1 shows a sketch of our experimental setup to measure the fractional-order moments in thermal light ghost imaging. The thermal light fields in the object plane and reference plane are represented by two identical sets of random speckles.

*Project supported by the National Natural Science Foundation of China (Grant Nos. 11674273, 11304016, and 11204062).
†Corresponding author. E-mail: dzcao@ytu.edu.cn
‡Corresponding author. E-mail: xin-bing.song@weizmann.ac.il
© 2018 Chinese Physical Society and IOP Publishing Ltd

The bucket detector D_B converts the total optical intensity out of the object, depicted by the letter "A", into the bucket signals I_B. The reference detector D_r scans in the reference plane and converts the local intensity into the reference signals I_r. In the experiment, the bucket detector and reference detector are two charge coupled devices. The correlator device is used to measure the fractional-order moments $\langle I_B^{\mu} I_r^{\nu} \rangle$. A screen shows the ghost image that is reconstructed from the fraction-order moments of the bucket and reference signals.

We synchronically divide the object and reference planes into n identical units, as shown in Fig. 1. We assume that: (i) all the units are small enough to maintain the object details,; (ii) the unit size is comparable with the resolving power of the thermal light ghost imaging, which is inversely proportional to the coherence length of the optical fields in the object and reference planes; and (iii) the thermal fields in all the units are statistically independent from each other.

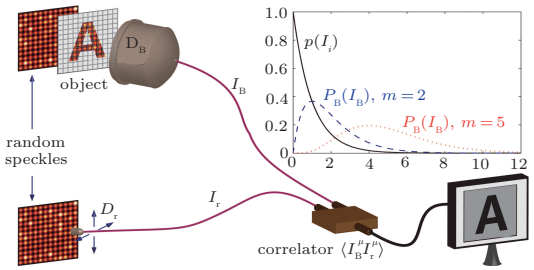


Fig. 1. (color online) A sketch of the experimental setup. The random speckles are two identical pseudo-thermal light beams. The upper is the object beam and the lower is the reference beam. D_B is the bucket detector, and the pixel detector D_r registers the reference beam. The fractional moments $\langle I_B^{\mu} I_r^{\nu} \rangle$ are performed by the correlator. The subplot shows the PDFs in Eq. (16) for $m = 1$, 2, and 5, where m is the number of the nonzero units in the object.

According to probability theory, we regard the thermal light intensities of the reference signals as a set of stochastic variables $I_r = \{I_1, I_2, \ldots, I_n\}$. Each element of the reference signals I_i ($i = 1, 2, \ldots, n$) independently meets the negative exponential probability distribution $p(I_i) = (1/I_0)\,\mathrm{e}^{-I_i/I_0}$, where the constant I_0 represents the intensity average.

The object is described by a column vector $T = \{t_1, t_2, \ldots, t_n\}'$, where the prime denotes matrix transposition, $0 \le t_i \le 1$ is the transmittance or reflectivity of the i-th object unit. The object signals can also be regarded a set of stochastic variables

$$Y = \{I_1 t_1, I_2 t_2, \ldots, I_n t_n\} = \{y_1, y_2, \ldots, y_n\}, \tag{2}$$

where $y_i = I_i t_i$ ($i = 1, 2, \ldots, n$). Therefore, the PDF of the variable y_i from the i-th object unit becomes

$$p_i(y_i) = \frac{p(y_i/t_i)}{t_i} = \frac{1}{I_0 t_i}\,\mathrm{e}^{-y_i/I_0 t_i}, \tag{3}$$

where $i = 1, 2, \ldots, n$. We can see from Eq. (3) that each variable in the object plane fulfills the negative exponential distribution, just with a modified average $I_0 t_i$. We note that the limitation of $p_i(y_i)$ becomes $\lim_{t_i \to 0} p_i(y_i) = \delta(y_i)$ when t_i tends to zero.

The bucket detector D_B collects all of the object beams. Therefore, the bucket signals can be described by a stochastic variable

$$I_B = \sum_{i=1}^{n} y_i = \sum_{i=1}^{n} I_i t_i, \tag{4}$$

which is a linear sum of n independent variables $\{I_i\}$ with corresponding weights $\{t_i\}$. Consequently, the PDF for the bucket signals is expressed by

$$P_B(I_B) = \mathscr{L}^{-1}_{s \to I_B} \left[\prod_{i=1}^{n} \widetilde{p}_i(s) \right], \tag{5}$$

where $\widetilde{p}_i(s)$ is the Laplace transformation of $p_i(x)$

$$\widetilde{p}_i(s) = \mathscr{L}_{x \to s}[p_i(x)] = \frac{1}{1 + (I_0 t_i)s}, \tag{6}$$

the symbol $\mathscr{L}_{x \to s}$ denotes the Laplace transformation from variable x to s, and $\mathscr{L}^{-1}_{s \to I_B}$ denotes the inverse Laplace transformation.

As shown in Eq. (4), each element I_i is in correspondence with the variable $y_i = I_i t_i$ of the bucket signal I_B. The joint PDF between the two variables, I_i and y_i, is $p(I_i)\delta(y_i - I_i t_i)$. Except for y_i, the other $n-1$ variables $\{y_j\}_{j \ne i}$ in the bucket signal (4) are statistically independent of the reference signal I_i. Thus, the joint PDF between the bucket signals I_B and the reference signal I_i is obtained as

$$P_2(I_B, I_i) = P'_B(I_B - I_i t_i) \times p_i(I_i), \tag{7}$$

where $i = 1, 2, \ldots, n$, and

$$P'_B(I'_B) = \mathscr{L}^{-1}_{s \to I'_B} \left[\prod_{j=1 (j \ne i)}^{n} \widetilde{p}_j(s) \right] \tag{8}$$

is the PDF of the variable $I'_B = I_B - I_i t_i$. Equations (4), (5), and (6) are taken into account in Eq. (7).

Obviously, the joint PDF $P_2(I_B, I_i)$ reflects the intrinsic relation between the bucket signals I_B and the reference signal element I_i. The joint PDF $P_2(I_B, I_i)$ can be separable only if $t_i = 0$. Another feature should be noted that PDFs of $P_B(I_B)$ in Eq. (5) and $P_2(I_B, I_i)$ in Eq. (7) do not depend on the specific distribution of the object but instead depend on the histogram of the object. In this paper, these PDFs form the probability theory basis of image reconstruction in correlated ghost imaging systems.

3. Fractional-order moments for ghost imaging

Since the reference signals meet negative exponential distribution $p(I_i) = (1/I_0)\,\mathrm{e}^{-I_i/I_0}$, it is clear that $p(I_i = 0) \ge p(I_i)$. The fractional-order moment of the reference signal is

$$\langle I_i^{\nu} \rangle = \int_0^{\infty} I_i^{\nu} \times p(I_i)\,\mathrm{d}I_i = \Gamma(1 + \nu) I_0^{\nu} \tag{9}$$

for any fractional number ν, where the Gamma function is

$$\Gamma(1+\nu)=\int_0^\infty t^\nu \mathrm{e}^{-t}\,\mathrm{d}t,$$

and $i=1,2,\ldots,n$. Since the largest probability of the reference signal lies at $I_i=0$, we should set ν positive ($\nu>0$) to avoid infinity.

As was proven previously, the bucket signals no longer meet the negative exponential distribution. Specifically, we consider a simple case that the object contains only two nonzero points $T=\{t_1,t_2\}'$, where $t_1>0$ and $t_2>0$. Both variables in $Y=\{y_1,y_2\}$ and Eq. (2) meet the probability density function in Eq. (3). Considering Eqs. (3) and (5), we obtain the PDF of the bucket signals as

$$P_\mathrm{B}(I_\mathrm{B})=\frac{\mathrm{e}^{-I_\mathrm{B}/I_0t_1}-\mathrm{e}^{-I_\mathrm{B}/I_0t_2}}{I_0(t_1-t_2)}. \tag{10}$$

We find $P_\mathrm{B}(I_\mathrm{B}=0)=0$. For trivial objects $t_1=t_2=t$, the PDF of the bucket signals is $P_\mathrm{B}(I_\mathrm{B})=(I_B/I_0^2\cdot t^2)\,\mathrm{e}^{-I_\mathrm{B}/I_0t}$. Similarly, it can be proven that $P_\mathrm{B}(I_\mathrm{B}=0)=0$ is always valid for more complicated objects than the two-point object. The fractional moment of the bucket signal is

$$\langle I_\mathrm{B}^\mu\rangle=\int_0^\infty I_\mathrm{B}^\mu\times P_\mathrm{B}(I_\mathrm{B})\,\mathrm{d}I_\mathrm{B}, \tag{11}$$

where μ can be any arbitrary fractional numbers since the probability $P_\mathrm{B}(I_\mathrm{B}=0)=0$ for any real object.

The fractional-order joint-moment in Eq. (1) between the bucket and reference signals now can be specifically written as

$$\langle I_\mathrm{B}^\mu I_i^\nu\rangle=\int_0^\infty \mathrm{d}I_\mathrm{B}\int_0^{I_\mathrm{B}/t_i}\mathrm{d}I_i\times I_\mathrm{B}^\mu I_i^\nu P_2(I_\mathrm{B},I_i). \tag{12}$$

The object information can be reconstructed by measuring the set of fractional-order moments

$$\langle I_\mathrm{B}^\mu I_r^\nu\rangle=\{\langle I_\mathrm{B}^\mu I_1^\nu\rangle,\langle I_\mathrm{B}^\mu I_2^\nu\rangle,\ldots,\langle I_\mathrm{B}^\mu I_n^\nu\rangle\} \tag{13}$$

in the TLGI experiments. For the same reason as mentioned previously, the fractional numbers in Eqs. (12) and (13) meet $\nu>0$ and $\mu\neq 0$.

We should pay more attention to the fractional-order moments $\langle I_\mathrm{B}^\mu I_i^\nu\rangle_0$ and $\langle I_\mathrm{B}^\mu I_i^\nu\rangle_1$ for $t_i=0$ and $t_i=1$, respectively. The former, in the case $t_i=0$, defines the background of the ghost images $\langle I_\mathrm{B}^\mu I_i^\nu\rangle_0=\langle I_\mathrm{B}^\mu\rangle\langle I_i^\nu\rangle$. Meanwhile, the latter, in the case $t_i=1$, $\langle I_\mathrm{B}^\mu I_i^\nu\rangle_1$ defines the correlation function in accordance with the highest value of the object. These fractional-order correlation functions meet

$$\langle I_\mathrm{B}^\mu I_i^\nu\rangle_{1(\mu>0)}>\langle I_\mathrm{B}^\mu I_i^\nu\rangle_0,\quad \langle I_\mathrm{B}^\mu I_i^\nu\rangle_{1(\mu<0)}<\langle I_\mathrm{B}^\mu I_i^\nu\rangle_0. \tag{14}$$

It is clear that the ghost image is above its background when $\mu>0$, and is below its background when $\mu<0$; that is, negative (positive) ghost images can be obtained for negative (positive) fractional orders μ.

Consequently, the visibility degree and peak SNR of the ghost images in fractional-order moments are defined as

$$V=\frac{\left|\langle I_\mathrm{B}^\mu I_i^\nu\rangle_1-\langle I_\mathrm{B}^\mu I_i^\nu\rangle_0\right|}{\langle I_\mathrm{B}^\mu I_i^\nu\rangle_1+\langle I_\mathrm{B}^\mu I_i^\nu\rangle_0},$$

$$R_\mathrm{p}=\frac{\sqrt{N}\left|\langle I_\mathrm{B}^\mu I_i^\nu\rangle_1-\langle I_\mathrm{B}^\mu I_i^\nu\rangle_0\right|}{\sqrt{\left|\left\langle I_\mathrm{B}^{2\mu}I_i^{2\nu}\right\rangle_1-\langle I_\mathrm{B}^\mu I_i^\nu\rangle_1^2\right|}}, \tag{15}$$

where N is the number of sampling in experiment, the symbol $|\cdots|$ is used to make the visibility and peak SNR compatible with both the positive and negative images.

In principle, the precise forms of the PDF $P_\mathrm{B}(I_\mathrm{B})$ and joint PDF $P_2(I_\mathrm{B},I_i)$ can be determined if the histogram of the object is given. The fractional moments $\langle I_\mathrm{B}^\mu I_\mathrm{r}^\nu\rangle$ can further be used to retrieve the object information. Later on, we show the experimental results of the fractional-order moments for binary objects in TLGI.

4. Experiment results with binary objects

To explicitly exhibit the probability theory method and to illustrate the characteristics of ghost images from fractional-order moments in TLGI, we consider the case of binary objects where the values of the object units are just $t_i=0$ or 1. From Eq. (5), the bucket signals meet Gamma distribution with PDF

$$P_\mathrm{B}(I_\mathrm{B})=\frac{I_\mathrm{B}^{m-1}}{(m-1)!I_0^m}\,\mathrm{e}^{-I_\mathrm{B}/I_0}, \tag{16}$$

where m is the number of the nonzero units in the object. The PDFs $P_\mathrm{B}(I_\mathrm{B})$ of Eq. (16) for $m=1$, 2, and 5 are plotted by the solid black, dashed blue, and dotted red lines, respectively, in the subplot of Fig. 1. The limitation of $\lim_{m=1}P_\mathrm{B}(I_\mathrm{B})\to p(I_i)$ is considered. We find that $p(0)\geq p(I_i)$ for the single-unit object and $P_\mathrm{B}(0)=0$ for a more complicated object. The joint PDF between the reference and bucket signals is

$$P_2(I_\mathrm{B},I_i)=\begin{cases}\dfrac{(I_\mathrm{B}-I_i)^{m-2}}{(m-2)!I_0^m}\,\mathrm{e}^{-I_\mathrm{B}/I_0}, & (t_i=1),\\ \dfrac{I_\mathrm{B}^{m-1}}{(m-1)!I_0^{m+1}}\,\mathrm{e}^{-(I_\mathrm{B}+I_i)/I_0}, & (t_i=0),\end{cases} \tag{17}$$

where $I_i\leq I_\mathrm{B}$ and $m\geq 2$.

The ensemble average of the reference signals is $\langle I_i\rangle=I_0$, and the ensemble average of the bucket signals is $\langle I_\mathrm{B}\rangle=mI_0$. From Eqs. (12) and (17) we obtain the fractional-order moments

$$\begin{aligned}\langle I_\mathrm{B}^\mu I_i^\nu\rangle_0&=\frac{\Gamma(m+\mu)\Gamma(1+\nu)}{\Gamma(m)}I_0^{\mu+\nu},\\ \langle I_\mathrm{B}^\mu I_i^\nu\rangle_1&=\frac{\Gamma(m+\mu+\nu)\Gamma(1+\nu)}{\Gamma(m+\nu)}I_0^{\mu+\nu}\end{aligned} \tag{18}$$

for $t_i=0$ and $t_i=1$, respectively.

Equation (18) presents the background and maximum of the image. Therefore, the quality of ghost images varies with the orders μ and ν. From Eqs. (15) and (18), the visibility degree and peak SNR of the ghost images are

$$V = \left| \frac{\Gamma(m+\mu+\nu)\Gamma(m) - \Gamma(m+\mu)\Gamma(m+\nu)}{\Gamma(m+\mu+\nu)\Gamma(m) + \Gamma(m+\mu)\Gamma(m+\nu)} \right|, \tag{19}$$

$$R_{\mathrm{p}} = \frac{\left| \frac{\Gamma(m+\mu+\nu)\Gamma(1+\nu)}{\Gamma(m+\nu)} - \frac{\Gamma(m+\mu)\Gamma(1+\nu)}{\Gamma(m)} \right|}{\sqrt{\frac{\Gamma(m+2\mu+2\nu)\Gamma(1+2\nu)}{N\cdot\Gamma(m+2\nu)} - \frac{\Gamma^2(m+\mu+\nu)\Gamma^2(1+\nu)}{N\cdot\Gamma^2(m+\nu)}}}, \tag{20}$$

respectively for binary objects. Therefore, the fractional orders provide more detailed parameters to exquisitely adjust or modify the image quality than the integer orders in practice.

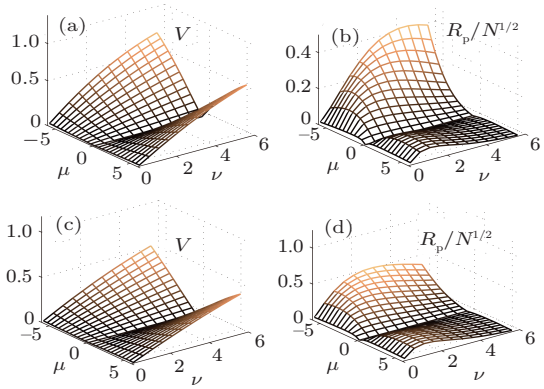


Fig. 2. (color online) Visibility degrees V [(a) and (c) and relative peak SNR $R_{\mathrm{p}}/\sqrt{N}$ [(b) and (d)] of binary objects. The object unit number (for $t_i = 1$) is $m = 20$ in panels (a) and (b), and $m = 30$ in panels (c) and (d).

The visibility degree V in Eq. (19) and the relative peak SNR $R_{\mathrm{p}}/\sqrt{N}$ in Eq. (20) versus the fractional orders are plotted in Fig. 2. The number of the nonzero units in the object is $m = 20$ in Figs. 2(a) and 2(b), and $m = 30$ in Figs. 2(c) and 2(d), respectively. We can see from Figs. 2(a) and 2(c) that the visibility degree increases as the absolute values of the correlation orders μ and ν increase. This result is similar to that in Ref. [17]. An evident feature is that the visibility degree of the negative image ($\mu < 0$) increases faster than that of the positive image ($\mu > 0$). Moreover, the greater number of the effective object units can degrade the visibility degree.

The relative peak SNRs are plotted in Figs. 2(b) and 2(d). The peak SNRs first increase and then decrease as the correlation orders $|\mu|$ and ν increase. We can also find that the maximum value of peak SNR of the negative image ($\mu < 0$) is greater than that of the positive image ($\mu > 0$). We can conclude that the image quality of the negative ghost images is better than that of the positive ghost images for the opposite fractional orders of $-\mu$ and μ. Furthermore, the visibility degree and SNR of the ghost image vary continuously with fractional (continuous) orders. Our method can help us to adjust the visibility degree and SNR at will by choosing appropriate experimental parameters.

In experiment, the pseudo-thermal light source is obtained by projecting a laser beam (laser diode: $\lambda = 650$ nm) onto a rotating ground glass plate[16] (which is not shown in Fig. 1). We set the diameter of the laser spot on the glass plate to be $d = 4.50$ mm, and the distance between the object and the glass plate to be $L = 8.50$ cm. The coherent length of the random laser speckles in the object plane is about $1.22\lambda L/d \simeq 14.98$ μm, which is smaller than the pixel pitch 20.0 μm of the charge coupled device. This ensures the well-performed thermal light ghost imaging, and fulfills the three assumptions proposed in Section 1.

Figure 3 shows our experimental results of the ghost images reconstructed from the normalized fractional-order moment

$$g_{\mathrm{i}}^{(\mu,\nu)} = \frac{\langle I_{\mathrm{B}}^{\mu} I_{\mathrm{i}}^{\nu} \rangle}{\langle I_{\mathrm{B}}^{\mu} \rangle \langle I_{\mathrm{i}}^{\nu} \rangle}. \tag{21}$$

A binary object, which contains $m = 373$ nonzero elements, is applied in our experiment. The number of the sampling is taken as $N = 1.2 \times 10^5$ in the experiment. The ghost images from the fractional-order moments are depicted in Figs. 3(a)–3(j) for $\mu = -16.5$, -12.5, -4.5, -1.5, -0.5, 0.5, 1.5, 4.5, 12.5, and 16.5, respectively. The parameter $\nu = 2.7183 \approx e$ is fixed in all the ghost images. We can see that the negative ghost images are obtained for negative orders $\mu < 0$ in Figs.3(a)–3(e). While the positive ghost images are obtained for positive orders $\mu > 0$ in Figs. 3(f)–3(j). The negative images distinguish our technique from that by the Boyd's group,[17,18] in which just positive integers of the correlation orders were considered.

Image quality also varies with the fractional orders. The visibility degrees V and peak SNRs R_p are listed in Table 1. The values of visibility degrees and peak SNRs are obtained by substituting the experimental data (N, $\langle I_B^{\mu} I_{\mathrm{i}}^{\nu} \rangle_1$, and $\langle I_{\mathrm{B}}^{\mu} I_{\mathrm{i}}^{\nu} \rangle_0$) in each image into Eq. (15). We find that the greater the absolute order $|\mu|$ is, the higher visibility degree of the ghost image becomes. In general, negative ghost images have better visibility than positive images. However, the behaviors of the peak SNRs differ greatly from that of the visibility degree. The approximate tendency of the peak SNRs for positive ghost images in Fig. 3 is that they decrease when $|\mu|$ increases. However, the peak SNRs of the negative ghost images first increase and then decrease when $|\mu|$ increases. This tendency is in accordance with the prediction of Fig. 2.

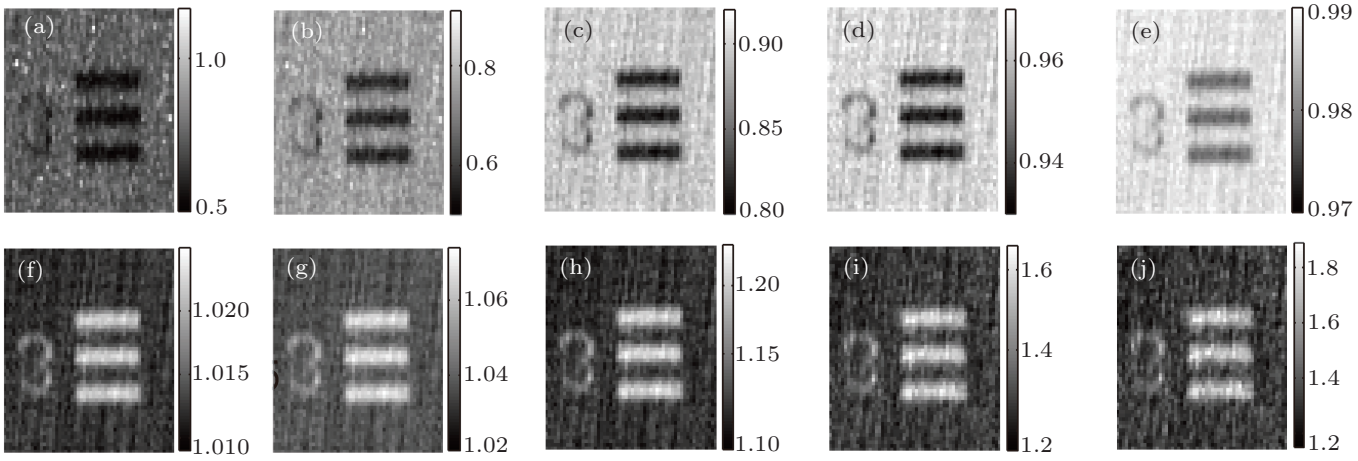


Fig. 3. Experimental results with binary objects. The ghost images are obtained from the normalized fractional-order moments in Eq. (21). The fractional orders are set $\mu = -16.5$ in panel (a), $\mu = -12.5$ in panel (b), $\mu = -4.5$ in panel (c), $\mu = -1.5$ in panel (d), $\mu = -0.5$ in panel (e), $\mu = 0.5$ in panel (f), $\mu = 1.5$ in panel (g), $\mu = 4.5$ in panel (h), $\mu = 12.5$ in panel (i), and $\mu = 16.5$ in panel (j). The parameter $\nu = 2.7183$ is fixed in all the ghost images. Each image has 56×56 pixels.

Table 1. Image visibility V and peak SNR R_{p} in Fig. 3.

Figure	3(a)	3(b)	3(c)	3(d)	3(e)	3(f)	3(g)	3(h)	3(i)	3(j)
μ	−16.5	−12.5	−4.5	−1.5	−0.5	0.5	1.5	4.5	12.5	16.5
V	0.4722	0.2608	0.067	0.0219	0.0073	0.0072	0.0215	0.0632	0.1778	0.2430
R_{p}	1.383	1.762	2.005	1.997	1.989	1.978	1.965	1.918	1.714	1.555

From these experimental results, we can see that our method of fractional-order ghost imaging has at least three distinguished features, compared with the methods of integer-order ghost imaging.[16–18] First, the fractional orders provides more detailed parameters than that in integer-order ghost imaging. These continuous parameters allow us to control the image quality in a more detailed way than the discrete integer orders. Second, the fractional-order ghost imaging produces negative images for negative correlation orders. The quality of the negative images is better than that of the positive images, in the cases that the fractional orders have the same absolute values. In the previous investigations, negative images do not exist in integer-order ghost imaging but they do exist in conditionally averaged ghost imaging.[21,22] Third, fractional-order ghost imaging gives a more universal theory than integer-order ghost imaging does. In other words, integer-order ghost imaging is a particular case of fractional-order ghost imaging. Our theory can predict all the behaviors of the integer-order ghost imaging.

5. Conclusions

In summary, we deduced the joint PDF between the bucket and reference signals. The joint PDF is the crucial step for us to investigate the fractional-order moments in TLGI systems. We found that the object information can be successfully reconstructed through measuring the fractional-order moments. The image visibility and peak SNRs varied with the fractional orders. We obtained negative (positive) ghost images for negative (positive) orders of the bucket signals. Our theory of fractional-order moments was illustrated in an experiment with a binary object. The positive and negative ghost images were successfully observed. When the absolute order of the bucket signals increases, the image visibility increases and the peak SNR of the positive image decreases. For negative images, however, their peak SNRs first increases and then decreases with the decreased orders.

Although our method was illustrated with binary objects in the experiment, it is also suitable for more complicated objects. The fractional-order moments show detailed correlation between the bucket and reference signals. These fractional orders provide wider parametric space than the integer orders do in thermal light ghost imaging. Although there is a long way to completely control the image quality in ghost imaging, the image visibility and SNR can now be adjusted to certain extent by choosing appropriate orders. We hope that our method provide an effective technique for signal processing.

References

[1] Bennink R S, Bentley S J and Boyd R W 2002 *Phys. Rev. Lett.* **89** 113601

[2] Cheng J and Han S 2004 *Phys. Rev. Lett.* **92** 093903

[3] Gatti A, Brambilla E, Bache M and Lugiato L A 2004 *Phys. Rev. Lett.* **93** 093602

[4] Valencia A, Scarcelli G, D'Angelo M and Shih Y 2005 *Phys. Rev. Lett.* **94** 063601

[5] Ferri F, Magatti D, Gatti A, Bache M, Brambilla E and Lugiato L A 2005 *Phys. Rev. Lett.* **94** 183602
[6] Zhang D, Zhai Y H, Wu L A and Chen X H 2005 *Opt. Lett.* **30** 2354
[7] Cao D Z, Xiong J and Wang K 2005 *Phys. Rev. A* **71** 013801
[8] Scarcelli G, Berardi V and Shih Y 2006 *Appl. Phys. Lett.* **88** 061106
[9] Basano L and Ottonello P 2006 *Appl. Phys. Lett.* **89** 091109
[10] Shapiro J H 2008 *Phys. Rev. A* **78** 061802
[11] Erkmen B I 2012 *J. Opt. Soc. Am. A* **29** 782
[12] Gong W, Zhao C, Yu H, Chen M, Xu W and Han S 2015 *Sci. Rep.* **6** 26133
[13] Wang C, Mei X, Pan L, Wang P, Li W, Gao X, Bo Z, Chen M, Gong W and Han S 2018 *Remote Sens.* **10** 732
[14] Clemente P, Durán V, Torres-Company V, Tajahuerce E and Lancis J 2010 *Opt. Lett.* **35** 2391
[15] Bertolotti J, van Putten E G, Blum C, Lagendijk A, Vos W L and Mosk A P 2012 *Nature* **491** 232
[16] Cao D Z, Xiong J, Zhang S H, Lin L F, Gao L and Wang K 2008 *Appl. Phys. Lett.* **92** 201102
[17] Chan K W C, O'Sullivan M N and Boyd R W 2009 *Opt. Lett.* **34** 3343
[18] Chan K W C, O'Sullivan M N and Boyd R W 2010 *Opt. Express* **18** 5562
[19] Terdik Gy, Woyczynski W A and Piryatinska A 2006 *Phys. Lett. A* **348** 94
[20] Consortini A and Rigalz F 1998 *Pure Appl. Opt.* **7** 1013
[21] Meyers R E, Deacon K S and Shih Y 2012 *Appl. Phys. Lett.* **100** 131114
[22] Luo K H, Huang B Q, Zheng W M and Wu L A 2012 *Chin. Phys. Lett.* **29** 074216